Gas and liquid-fuelled HVOF spraying of Ni50Cr coating: Microstructure and high temperature oxidation

B. Song, Z. Pala, K.T. Voisey, T. Hussain

PII: S0257-8972(16)30638-7
DOI: doi: 10.1016/j.surfcoat.2016.07.046
Reference: SCT 21376

To appear in: *Surface & Coatings Technology*

Received date: 1 April 2016
Revised date: 29 June 2016
Accepted date: 14 July 2016

Please cite this article as: B. Song, Z. Pala, K.T. Voisey, T. Hussain, Gas and liquid-fuelled HVOF spraying of Ni50Cr coating: Microstructure and high temperature oxidation, *Surface & Coatings Technology* (2016), doi: 10.1016/j.surfcoat.2016.07.046

Gas and liquid-fuelled HVOF spraying of Ni50Cr coating: microstructure and high temperature oxidation

B. Song, Z. Pala, K.T. Voisey and T. Hussain
Faculty of Engineering, the University of Nottingham, NG7 2RD, UK

Abstract

Ni50Cr thermally sprayed coatings are widely used for high temperature oxidation and corrosion in thermal power plants. In this study, a commercially available gas atomised Ni50Cr powder was sprayed onto a power plant alloy (ASME P92) using both gas and liquid fuelled high velocity oxy-fuel (HVOF) thermal spray. Microstructures of the two coatings were examined using SEM- EDX, XRD, oxygen content analysis and mercury intrusion porosimeter. The gas fuelled coating had higher levels of oxygen content and porosity. Shorter term air oxidation tests (4 h) of the free-standing deposits in a thermogravimetric analyser (TGA) and longer term air oxidation tests (100 h) of the coated substrates were performed at 700 ℃. The kinetics of oxidation and the oxidation products were characterized in detail in SEM / EDX and XRD. In both samples, oxides of various morphologies developed on top of the Ni50Cr coatings. Cr_2O_3 was the main oxidation product on the surface of the coatings along with a small amount of NiO and $NiCr_2O_4$. Rietveld analysis was performed on the XRD data to quantify the phase composition of the oxides on both Ni50Cr coatings and their evolution with time.

Keywords: HVOF, Ni50Cr, liquid fuel, gas fuel, microstructure, oxidation

1. Introduction

The use of a suitable corrosion resistant coating is an economically attractive approach to solving the high temperature oxidation and corrosion problem for power plant heat exchanger materials and turbines. In recent years, there has been a growing interest in the use of high velocity oxy-fuel (HVOF) thermal spraying for deposition of protective coatings onto power plant alloy substrates [1-6]. In the HVOF process, oxygen and a fuel (gas/liquid) are mixed in the combustion chamber of a spray gun and the feedstock material is injected into the chamber by a carrier gas stream. Consequently, the injected powder particles are rapidly heated and accelerated towards the substrate, achieving velocities of the order of 450 - 1200 m s^{-1} before impact [7]. In HVOF spray, powder particle temperatures are relatively low and particle velocities are relatively high in comparison with other thermal spraying processes, such as air or vacuum plasma spraying [7]. It is therefore possible to minimize the decomposition of the feedstock during spraying by careful control of processing parameters and obtain high quality, low oxygen content and low porosity coatings which are well bonded to the substrate. HVOF thermal spraying mainly includes two types of fuel: gas (hydrogen, methane, propane, propylene, natural gas etc.) and liquid (kerosene, etc.). Typically, the liquid fuelled HVOF spraying can obtain a higher spray rate, while the gas fuelled HVOF spraying can achieve higher deposition efficiency [8]. The in-flight oxidation of the particles is also different, since the temperature of the flame in the HVOGF gun is usually higher than that in the HVOLF gun. In a thermal sprayed coating, interconnected porosity, oxide-containing splat boundaries, voids formed at the splat boundaries and inhomogeneous composition, all affect the high temperature oxidation performance of the coatings [3]. These above features can vary in coatings manufactured from the same feedstock powder but through different HVOF thermal spraying techniques [4-6, 9].

Among commercially available coating materials, NiCr based alloys are widely used to provide corrosion resistance at elevated temperatures since the selective oxidation of Cr can

form a slowly growing protective layer [10]. Previous studies have shown that HVOF thermal sprayed NiCr based coatings can provide acceptable protection to power plant substrates from high temperature corrosion. For instance, Oksa, *et al.* [2] examined the corrosion performance of HVOF sprayed NiCr16Mo, NiCr9Mo and NiCr10Al coatings in a biomass boiler conditions for two years and found that all those three coatings have excellent corrosion performance. They also indicated that corrosion in HVOF sprayed coatings typically occurs through oxidized lamellar boundaries and pores in the coating, i.e. pore-free and less oxidised microstructure provided superior performance. Bluni *et al.* [3] also obtained similar results using HVOF sprayed NiCr coating in coal fired combustion environment (environment containing SO_2 rather than Cl_2). Studies from other researchers also indicate that NiCr based coating can provide excellent protection in high temperature corrosion.

According to the Ni-Cr binary phase diagram [11], chromium is soluble in nickel up to a maximum of 47 wt.% at the eutectic temperature which drops off to around 30 wt. % at room temperature. Since chromium is the main element which could form oxide scale, its solubility in matrix is important for corrosion resistant alloys. Oxidation resistance of NiCr alloy can be attributed to the formation of a highly adherent protective scale, in which the diffusion rate of oxygen is reduced [10]. The oxide scale thus formed in a Ni-Cr alloy is a mixture of nickel and chrome oxides (NiO, Cr_2O_3 and $NiCr_2O_4$) [10]. In general, oxidation and corrosion resistance of Ni-Cr alloys increase with increasing the levels of chromium [9, 12]. Ni50Cr powder is a commercially available feedstock with high Cr content that was developed for high temperature applications.

In the present study, a gas atomized Ni50Cr feedstock powder was sprayed onto a power plant alloy using both gas and liquid fuelled high velocity oxy-fuel (HVOF) thermal spray. The oxygen content and porosity of the coating were investigated. Short term and long term high temperature oxidation tests were conducted to examine the oxidation behaviour of deposited

coatings. SEM/ EDX and XRD were all used to identify the phase changes during the high temperature oxidation.

2. Experimental

2.1 Materials: substrate and feedstock powder

Gas atomised Ni50Cr powder (1260F/Ni-980-1) supplied by Praxair surface technology Ltd (Germany) with a size range of -53 +20 μm was used in these spray trials. Small coupons of 60 × 20 × 2 mm were machined from a 9 Cr ferritic martensitic boiler grade steel (ASME P92) pipe sections and used as a substrate material for both spray trials. Before deposition these plates were grit blasted with brown alumina and degreased with isopropyl alcohol to improve substrate surface roughness and eliminate contaminants respectively. Compositions of substrate and powder are provided in Table 1.

2.2 Coating deposition

Two HVOF systems were utilized to deposit the Ni50Cr powder onto the boiler steel substrate: One is a HVOGF (High Velocity Oxy Gaseous Fuel) setup and the other one is a HVOLF (High Velocity Oxy Liquid Fuel) setup. Schematic diagrams of the two kinds of HVOF gun are shown in Figure 1. In this study, the HVOGF setup comprises of a Top Gun thermal spraying system (GTV Verschleiss-Schutz GmbH, Germany) with a powder feeder and gas control console. As shown in Figure 1 (a), the HVOGF gun operates as follows: powder is fed axially into the rear of the combustion chamber where oxygen and fuel (hydrogen) are mixed and combusted. The hot gas and entrained powder are then accelerated through the combustion chamber and down the parallel sided nozzle, which is approximately 220 mm long, before emerging as a free jet [13]. The HVOLF setup comprises of a Met Jet III system (Metallisation Limited, Dudley, UK) and a schematic setup is displayed in Figure 1 (b). In this gun, kerosene and oxygen are fed into the combustion chamber where kerosene is vaporised, mixed with oxygen and the mixture burns before passing through the converging-

diverging throat which accelerates the gas to a Mach number between 1.5 and 2. Powder is fed radially into the gas stream through two ports which are located downstream of the throat. The gas and entrained powder then flow along the nozzle, before emerging as a free jet [13]. To deposit coatings onto P92 substrates flat coupons were mounted vertically on the circumference of a turntable with a vertical axis of rotation and the spray gun was positioned at the front of the rotating coupons at a fixed stand-off distance to give a horizontal spraying jet. This setup has been adopted by pervious researcher [7]. Detailed spraying parameters had been optimized and are listed in Table 2. Freestanding coatings were produced by spraying onto ground substrates, which were carefully shaped around a mandrel to delaminate the coatings from the substrate.

2.3 High temperature oxidation exposure of specimens

To obtain the oxidation kinetics of the coatings, free-standing coatings were investigated in a thermogravimetric analyser (TGA) (TA instruments Q600, Herts, UK). To prepare the samples for TGA analysis, a square section of dimensions approximately 3 x 3 x 0.2 mm was cut from a freestanding coating using a precision diamond tipped cutting disk. The specimens were cleaned using industrial methylated spirit, dried and weighed using a precision balance (± 0.0001 g). The total surface area of each of the TGA samples was also measured using a micrometer to an accuracy of ± 1 μm. The oxidation tests were then carried out in commercial grade bottled air (flow rate of 20 mL min^{-1}) at 700 ℃. Samples were held in a recrystallized alumina pan and heated at a rate of 5 ℃ min^{-1} to the test temperature. They were maintained at the test temperature for 4 hours before being cooled down to room temperature, also at a rate of 5 ℃ min^{-1}. The TGA data was corrected to take into account of the weight change data when the sample reached the target test temperature.

The longer term air oxidation exposure was carried out in a box furnace (Lenton ECF 12/6, Lenton Thermal Design Ltd., UK). The coated samples were placed in individual crucibles

made from high-density alumina and the tests were carried out at 700 ℃ for 1, 10 and 100 h with a heating rate of 6 ℃ min^{-1}. At the end of the test cycle the samples were furnace cooled to room temperature also at a rate of 6 ℃ min^{-1}.

2.4 Specimens characterization

Feedstock powder particles and as-sprayed coatings were mounted in a conductive resin, ground and polished to a 1 μm diamond finish for the scanning electron microscope (SEM) examination. The samples were cut using a diamond tipped precision cutting saw to analyse the coating cross-sections. The exposed samples were cold mounted with a low shrinkage resin filled with glass bids to protect the oxide scale before preparing to a 1 μm diamond finish. All microstructure investigation was performed in a FEI field emission gun SEM (FEI, Eindhoven, Netherland) at 20 kV. The morphology of oxide scales at the top of coatings was then examined in the SEM using secondary electron (SE) signal while the cross-section of the samples was examined using backscattered electron (BSE) signals. Energy dispersive x-ray (EDX) analysis was carried out to characterize the oxide scales and the composition of the coatings.

Powder, as-sprayed and heat treated coatings were also investigated in an x-ray diffraction (XRD) using a Siemens D500 diffractometer employing monochromatic Cu Kα with a wavelength of 0.15406 nm radiation. XRD scans were performed between 10- 90º with a 2θ step size of 0.05º and a dwell time per step of 5s. The Rietveld method was used on the XRD data to identify the phase fractions, which is a full-profile approach that was initially introduced for the refinement of crystal structure parameters but has been expanded for application in quantitative phase-analysis over the last several decades [14].

The oxygen content of the as-sprayed coatings was measured with Leco oxygen analyser (Leco ON736, LECO Instruments UK Ltd, Stockport, UK). Leco oxygen contents analysis utilized a combustion method to determine the small content of oxygen in samples. The

samples are placed into a pure graphite crucible and heated under a flowing stream of helium and the combustion gases are measured through infrared absorption and thermal conductivity. During this process, oxygen and carbon combine to form CO_2. The content of oxygen in the sample can be calculated according to the amount of produced CO_2. Both HVOGF and HVOLF free-standing coatings were measured three times to get an average.

The porosity of the free-standing coatings was measured with a mercury intrusion porosimeter (MIP) (AutoPore IV 9500, Micrometrics, Micrometrics UK Ltd., Hexton, UK). Mercury intrusion porosimeter utilizes the unique properties of mercury. Since mercury does not wet most substances and it does not spontaneously penetrate pores by capillary action, it must be forced into the pores by the application of external pressure. The required equilibrated pressure is inversely proportional to the size of the pores, only slight pressure being required to intrude mercury into large macropores, whereas much greater pressures are required to force mercury into small pores.

3. Results

3.1 Microstructure of powder and as-sprayed coatings

XRD patterns of the Ni50Cr feedstock powder, the HVOGF and HVOLF coatings are shown in Figure 2. The powder pattern comprises three main peaks (2θ = 43.5º, 51º and 76º) corresponding to the fcc γ - (Ni, Cr) solid solution and three minor peaks (2θ = 45º, 65.5º and 83º) corresponding to the bcc α-Cr. The position of these main peaks shifted slightly left in the diagram compared to that of pure fcc Ni phase peaks due to the expansion effect of the Cr atom in the lattice of Ni, which is brought about by the rapid cooling of (Ni, Cr) super-saturation solution during gas atomization process. From the XRD pattern of feedstock powder it was deduced that there were no oxide phases or at least the volume fractions of any oxides phases were below the limit of detection. Figure 3 (a) shows the morphology of the as-received powder particles in secondary electron imaging. This image shows the typical

powder morphology of the inert gas atomized powders since most particles were near-spherical. It also reveals that there are some smaller satellite particles around larger particles. The polished cross-section image of a power particle shows a dendritic solidification pattern as a consequence of gas atomisation (Figure 3 (b)).

For the HVOGF as-sprayed coating, there are several oxide phases as can be seen from corresponding XRD patterns. The oxides phases include NiO, $NiCr_2O_4$ spinel and Cr_2O_3. It appears that NiO ($2\theta = 38^o$ and 63.5^o) and $NiCr_2O_4$ ($2\theta = 18.5^o$, 31^o, 36^o, 57.5^o and $64.5\ ^o$) are two major oxidation products in the HVOGF as-sprayed coating, since the intensity of their peaks is much larger than those of Cr_2O_3. The α-Cr phase could not be detected in the HVOGF sprayed coatings, instead, three new peaks ($2\theta = 44^o$, $52\ ^o$ and 76.5^o) corresponding to Ni phase were identified. The XRD pattern of the as-sprayed HVOLF coating shows identical peak positions to that of the powder, indicating there are no new phases appeared during the spraying process. The two minor α-Cr peaks ($2\theta = 65.5^o$ and 83^o) were not clearly detected in in the HVOLF coating. It should be noted that no oxide peaks were detected in the XRD pattern of the HVOLF as-sprayed coating within the detection limit of the XRD (1- 2 % wt) [15].

Figure 4 shows the BSE images of the cross-section of both the coatings on P92 substrate. The HVOGF as-sprayed coating as shown in Figure 4 (a) is around 130 μm in thickness and shows a good coating-substrate interface without any delamination or crack at the interface. Large deformation of the lamellar splats is the most obvious feature of this coating microstructure. The black features surround the splats are oxides according to the EDX analysis in Figure 4 (b). The higher magnification image in Figure 4 (b) shows a globular pore marked by an arrow. The amount of oxidation of the powder particles during the spraying process is significantly high, which has been measured by the LECO infrared oxygen contents analysis. The level of oxygen in this coating was detected to be around 8.66 wt %.

Powder particles in the as-sprayed HVOLF coating (Figure 4 (c) and (d)) experienced little oxidation and deformation when compared to the microstructure of the as-sprayed HVOGF coating. The lamellar splats were hemispherical in shape and a thin layer of oxide surrounds the splats (appears darker in contrast in the BSE images of Figure 4 (c) and (d)). The coating was around 200 μm in thickness and again no delamination or crack at the interface was observed. A small amount of porosity within the coating is observed at the top layer (up to 40 μm from the top surface) and there is almost no porosity below this level. The dendritic pattern observed in the feedstock powder particles (Figure 3 (b)) was still retained after thermal spraying (Figure 4 (d)), indicating that the powder particles in the HVOLF thermal spraying gun did not undergo complete melting. The oxygen content of the as-sprayed coating was only 0.464 wt. %, much lower than that of HVOGF as-sprayed coating.

The top surface of the as-sprayed coating was also examined in SE imaging mode and shown in Figure 5. For the HVOGF as-sprayed coating, no un-melted particles were observed; the deformation of powder particles during spraying is quite significant. While for the HVOLF as-sprayed coating, there are a large amount of un-melted particles on the surface, which has hemispherical morphology. This is representative of the coatings morphology typically observed in the HVOLF spraying, where the particles are not fully molten.

3.2 Porosity of as-sprayed coatings

MIP is the most accurate method to provide the size distribution of pores and volume percentage of open porosity. This information is quite useful in evaluating oxidation performance of coatings since pore inside the HVOF coatings is the main transport path of oxygen ion [9]. Diffusion of oxygen ions and other corrosive species is much faster in pores than in metal and oxide scale [3]. Incremental intrusion of mercury vs. pore sizes in both as-sprayed coatings is plotted in Figure 6. The size distribution of pores inside the HVOGF coating is much wider and randomly distributed from 0.01 μm to 40 μm. The size distribution

of pores inside the HVOLF coating falls in two small ranges, i.e., between 10 - 30 μm and 0.006 - 0.3 μm. Figure 7 shows the cumulative intrusion of mercury vs. pore sizes for both coatings. HVOGF coating has a larger cumulative intrusion (0.006 ml g^{-1}), which is almost twice of that of HVOLF coating (0.003 ml g^{-1}). Ignoring the oxides in the coating, the cumulative intrusion of mercury can be converted to volume percentage of porosity knowing the density of the feedstock material. Taking the density of the feedstock powder 8.2 g cm^{-3}, the porosity of HVOLF coating was around 2.46 vol. % and the porosity of the HVOGF coating was 4.92 vol. %.

3.3 High Temperature Oxidation

3.3.1 Oxidation Kinetics: TGA

The free-standing coatings were examined in a TGA in laboratory air for 4 h at 700 ℃ and the results are shown in Figure 8. Mass gain of the HVOGF sample was about 0.166 mg cm^{-2} after 4 h, while the mass gain of the HVOLF sample was 0.132 mg cm^{-2}. The square of the specific mass change vs. time was plotted in Figure 9 to determine kinetics of oxidation. Two straight lines can be fitted into each curve with satisfactory coefficient of determination. For HVOGF coating, the gradient of straight line at first stage is 2×10^{-4} $mg^2\,cm^{-4}\,min^{-1}$ which reduces to 8×10^{-5} $mg^2\,cm^{-4}\,min^{-1}$ at the consequent stage of oxidation. For HVOLF coating, the first stage of oxidation ends at around 60 minutes and the gradient of the corresponding straight line is 1×10^{-4} $mg^2\,cm^{-4}\,min^{-1}$, half of that of HVOGF coating. At the second stage of oxidation, the gradient decreases to 6×10^{-5} $mg^2\,cm^{-4}\,min^{-1}$, which is also less than that of HVOGF coating.

3.3.2 Oxidation products, morphology and cross-section

XRD patterns of the oxidation products after high temperature air exposure for various time period (1, 10 and 100 h) are shown in Figure 10 (HVOGF coating) and Figure 11 (HVOLF coating) respectively. The evolution of the phases with time was calculated using the Rietveld

method according to the XRD patterns for both coatings and the results are listed in Table 3. As can be seen from Figure 10 and Table 3, for HVOGF sprayed coating, the metallic phases included γ - (Ni, Cr) solid solution phase and fcc Ni phase. The γ - (Ni, Cr) increased from 28.1 wt. % in the as-sprayed coating to around 40.4 wt. % after 1 h exposure and the content of this phase was retained to a similar level after 100 h. Meanwhile, the Ni phase steadily decreased with increasing exposure time. Evolution of oxide phases includes a nine fold increase in Cr_2O_3 phase and a significant decrease of NiO and $NiCr_2O_4$ phases. For the HVOLF sprayed coating (Figure 11), the evolution of metallic phases with time is relatively complex. The α-Cr phase increased initially after 1 h and 10 h heat treatments but it was not detected after 100 h. There are no Ni phases in the initial as-sprayed coating; however, the phase was detected in the sample heat treated for 10 and 100 hours. The main metallic phase of γ- (Ni, Cr) decreased to about 43 wt. % after 100 h. Development of the NiO and $NiCr_2O_4$ in the HVOLF sprayed coating occurred at the later oxidation stages. Despite the differences in the evolution of the oxidation process of the two coatings, the compositions of oxidation products after 100 h are rather similar taking into consideration of the error of the Rietveld method.

Figure 12 (a-d) shows the SE images of the top morphology of the oxide grains after 100 h exposure in air for both coatings. Lower magnification images (5000×) show homogeneous coverage of the oxides on the surface of both HVOGF and HVOLF coatings. The geometry and size of oxide grains were examined at higher magnification (20000×) to study the nature of the oxide growth. As can be seen, the oxide grains developed after 100 h at the surface of HVOGF coating are much smaller. While in the HVOLF coating, the oxides have transformed into large well-defined grains. Typical size of the oxide grains was about 2 μm. EDX examination of lamellar oxide grains at the surface of two coatings show obvious differences. Oxide lamellar of the HVOGF coating includes more Ni element than those of HVOLF

coating (spectrum 1: 43 wt. % O, 1 % Si, 45 % Cr, 1 % Ni and spectrum 2: 45 wt. % O, 54.5 % Cr, 0.5 % Ni).

Cross-section images of both HVOGF and HVOLF coatings after air oxidation for 100 h are shown in Figure 13. A thicker oxide scale (3 - 5 μm) formed on the HVOGF coating (Figure 13 (b)) and a continuous thin oxide scale (1 - 2 μm) formed on the HVOLF coating (Figure 13 (e)). Although it is difficult to distinguish the grey level contrast between locations 1 and 2 in Figure 13 (b), the compositions are different; spectrum 1 contains 30 wt. % O, 1 % Si, 56% Cr, 12% Ni and Fe balance, spectrum 2 contains 29 wt. % O, 1% Si, 47 % Cr, 23 % Ni and Fe balance. A higher magnification image of the HVOGF coating cross-section is shown in Figure 13 (c). The BSE contrast in the image shows darker Cr rich regions and brighter Ni rich phases in the microstructure. On the other hand, the HVOLF coating after 100 h heat treatment shows a clear two phase microstructure (Figure 13 (f)): a Cr rich dark phase in a lighter Ni-Cr matrix. The HVOLF coating (Figure 13 (e)) following 100 h exposure show the following composition at spectrum 3: 24 wt. % O, 4 % Si, 47% Cr, 25% Ni and Fe balance. This is predominantly a chromia rich oxide with Ni. Besides, the inter-splat oxide at spectrum 4 has the following compositions: 14 wt. % O, 3% Si, 37% Cr, 45% Ni and Fe balance, which also shows that there are large differences between the inter-splat and surface oxides. A Cr depletion area was also noticed in the HVOLF coating, underneath the surface oxide, due to the selective oxidation of Cr at the coating surface (Figure 13 (f)).

4. Discussion

4.1 Microstructure and porosity of the coatings

The feedstock powder contains a range of particle sizes and these particles follow different trajectories through the gas steam during spraying. In HVOF thermal spraying, some particles will arrive in semi molten, molten and others in fully solid condition [7]. Extensive deformation of the particle will occur if the particle arrives in a semi-molten state, whereas,

fully solid particles will be more difficult to deform plastically. In HVOGF coating, the splats were mostly lenticular as a result of extensive melting and deformation upon impact. Metallic splats were 5-15 μm thick, which are separated by 1-2 μm thick oxide sheets. Hewitt calculated the flame temperatures and the excess oxygen in the flame for a range of gases and oxygen to fuel ratio [16]. The combustion of hydrogen and oxygen can theoretically reach 3123 K [16] and the melting temperature of Ni50Cr according to the phase diagram is 1618 K [11]; albeit, the particle temperature in the spray plume will depend on the residence time and the size of the particles.

The coating built up in HVOLF is similar to that described in the HVOGF spraying, but with a reduced degree of particle melting. The degree of particle melting depends on the size range of the particles. It is generally accepted that the particle bonding in HVOLF is better since a significant proportion of particles from the powder arrive at unmolten state [13]. In HVOLF, the particles are injected directly into a supersonic high temperature jet whereas in the HVOGF particles entre the slow, subsonic gas before being accelerated down the nozzle. As a result, the residence time of the particles in HVOLF is shorter and the particles are exposed to lower gas temperatures. Consequently, only a thin shell at the surface of the powder particles is melted in HVOLF, whereas a much larger proportion of a particle will melt in HVOGF (for a given particle size). This high degree of melting also resulted in higher oxidation of the HVOGF coating. Although, the coating was sprayed at 80 % oxygen stoichiometry, there is still excess oxygen in the flame due to decomposition of the combustion products at high temperature and turbulent mixing of the gas steam with air [7].

The degree of particle melting can explain the differences in the porosity measured by MIP. MIP is the most accurate means of measuring porosity of the thermal sprayed coatings and it has shown significant advantage over image analysis techniques in detecting sub-micron pores [17, 18]. The porosity of the coating > 10 μm was due to the surface roughness of the

coating (see Figure 5). The higher level of porosity in the HVOGF coating is attributed to the poor inter-splat bonding and localised pinhole pores in the coating. In HVOLF coating, the porosities were mostly in the range of 0.007 - 0.03 μm and these pores are mostly present at the inter-splat boundaries. A typical powder particle in thermal spraying comprises of a fully molten liquid shell, a solid unmolten core and a semi-solid region due to temperature gradient formation [13]. This liquid shell can react with oxygen in the flame and results in oxides in the coating. The inter-splat bonding also relies on this liquid shell and submicron porosities can arise when the particles are not packed well.

In the XRD scan of the HVOGF, significant peak broadening of the main fcc peaks was observed in the coating compared to the gas atomised powder. Peak broadening in thermal spraying is generally attributed to microstrain and fine grain size. Both of these factors are present in both the coatings. The microstrain in the HVOLF is probably higher due to the solid particle impact. Ni peaks appear in the HVOGF XRD scan due to the reduced alloying content of the coating. The Ni peak also correlates with the presence of Cr_2O_3 and the $NiCr_2O_4$ oxides found in the coating. Zhang *et al.* [13] reported that during the heating of the powder the alloying element Cr is preferentially oxidised from the fully molten zone where the mass transport is very high. $NiCr_2O_4$, NiO and Cr_2O_3 are formed on the particle surface, leaving a Cr depleted liquid droplet which solidifies on impact of the particle with the substrate. Indeed, this was observed in the EDX scans where the centre of the splats contained more Cr than the periphery of the splats. Numerical models indicate that small particles follow the gas temperature and velocity more closely and therefore reach higher temperatures [7]. It is evident from the microstructure that the particles become hot enough to melt. Molten particles are covered with an oxide skin and the oxidation of Cr and other elements proceed relatively slowly from the liquid. If the oxide film ruptures the oxidation will proceed more rapidly. The melting point of Cr_2O_3 is 2713 K and it is clear that only the smallest particles will reach this temperature. SEM and laser diffractometer data shows a large number of the

powder particles below sub ten micron and these could account for the formation of Ni rich regions in the coating. With regards to the composition of the oxide phase it is clear that the principal oxide phase was $NiCr_2O_4$ with small amount of Cr_2O_3 and NiO. The Ellingham diagram data on the free-energies on the formation of oxides shows the thermodynamic stability of oxides will increase from Ni to Cr. NiO, $NiCr_2O_4$ and Cr_2O_3 can all form in Ni-Cr based alloys but spinel is thermodynamically favoured at higher oxygen partial pressure and both Cr_2O_3 and spinel have been reported to form in initial, transient oxidation [7].

4.2 Kinetics of high temperature oxidation

It was not possible to fit a single straight line in the specific mass change squared vs. time plot for either of the coatings as the oxidation kinetics was composed of two separate mechanisms. Two straight lines were fitted into the curves in Figure 9 suggesting a two stage parabolic oxidation behaviour [10]. A number of allows at high temperature show a two stage oxidation behaviour, such as a two stage parabolic oxidation kinetic behaviour was reported in Ni20Cr alloy by Calvarin *et al.* [19]. The parabolic law indicates that the coatings developed a protective oxide layer with exposure time; hence, it can protect the underlying substrate from further oxidation. When assessing the oxidation performance of HVOF sprayed coating using mass change per area, error of this method should not be neglected: it is difficult to calculate the true surface area which actually contacts with the oxidizing atmosphere due to the surface roughness and porosities of as-sprayed coating; the oxides present within the as-sprayed coating (thin shell around splats) develop as well as new oxide nucleates on the total coating surface. Nonetheless, the lower parabolic rate constants for both stages for HVOLF coating show that the coating can provide a better oxidation resistant to the substrate than HVOGF coating. The transition in oxidation mechanisms occur in HVOLF coating after 60 minutes, whereas, the second stage in HVOGF coatings starts after 120 minutes. According to the XRD data, the main oxidation product after 1 h in HVOLF coating is Cr_2O_3, therefore, the first stage of oxidation is related to the formation of this oxide. After 10 h, oxidation product

such as $NiCr_2O_4$ was detected in the air oxidation sample; hence, it is believed that the second stage of oxidation kinetics after 60 mins is a combination of formation of chromia and Ni-Cr spinel oxides.

Oxidation kinetic studies of bulk Ni20Cr and Ni25Cr have been reported in literatures which can be compared with the oxidation behaviour of the coating in this study. Calvarin *et al.* [19] reported a two stage oxidation kinetic behaviour of Ni20Cr at 700 °C. The first stage obeys a parabolic law and the second stage follows a complete law (with a linear and parabolic component). The rate constant for Ni20Cr at 700 ℃ were 3.8×10^{-4} mg^2 cm^{-4} min^{-1} for the first stage and 2.6×10^{-7} mg^2 cm^{-4} min^{-1} for the second stage. Another study [20] reported the oxidation kinetic of Ni25Cr in the atmosphere Ar-20% O_2 at 1100 ℃, which is 1.66×10^{-4} mg^2 cm^{-4} min^{-1}. Values in this study for HVOF coatings (10^{-4} - 10^{-5} mg^2 cm^{-4} min^{-1}) are broadly in line with those reported data. Surface microstructure of the HVOF thermal sprayed coating is different from the bulk alloys, so some degree of variation is expected. Oxidation resistance of Ni50Cr coating obtained in this study is no less than that of Ni20Cr and Ni25Cr bulk alloy, which may indicate that high chromium NiCr alloy coating can provide satisfactory high temperature performance even it is manufactured using thermal spray.

4.3 Mechanism of oxidation of the Ni50Cr coating

During high temperature oxidation of nickel based high chromium system; there is a unique transient oxidation process [21]. In a Ni-20Cr alloy, both NiO and Cr_2O_3 are formed and grow laterally covering the entire surface. NiO grows faster than Cr_2O_3 but as previously mentioned the Cr_2O_3 is thermodynamically more stable than NiO [19]. Since the Ni-containing oxides grow much more rapidly than Cr_2O_3 a significant amount of NiO and $NiCr_2O_4$ can form before a continuous Cr_2O_3 layer can form. Among them $NiCr_2O_4$ is generated by reaction of NiO and Cr_2O_3 as shown in following reaction equation:

$$NiO + Cr_2O_3 \rightarrow NiCr_2O_4$$

As a consequence, a thin continuous layer of Cr_2O_3 forms near the metal surface and an outer $NiCr_2O_4$ in Ni-20Cr alloys. However, with increasing Cr content selective oxidation of Cr takes place and the formation of NiO is suppressed. The shift towards a single-phase Cr_2O_3 scale occurs at chromium content around 30 wt. % [22].

Before discussing the evolution of the oxides in the coatings, the x-ray penetration depth of the samples needs to be considered. The calculated penetration depth of x-rays into the Ni50Cr and Cr_2O_3 phases is around 2 - 7 μm according to the mass absorption coefficients of solids [15]. Thus, when discussing the oxide evolution process calculated using the Rietveld method, thickness of oxidation scale cannot be neglected. The as-sprayed HVOGF coating was mainly composed of γ and Ni phase, which transformed toward a γ rich phase with increasing heat treatment time. The Ni peak at 44.5° (2θ) disappeared only after 1 hour of heat treatment and the γ peak broadened as a consequence. The ratio of Ni to γ phases decreased as a function of the heat treatment time. A large quality of $NiCr_2O_4$ was found during spraying which decomposed to NiO and Cr_2O_3 only after 1 h of heat treatment. Chromium has higher affinity for oxygen than Ni and Cr forms more stable oxide and NiO is less stoichiometric oxide than Cr_2O_3 [23]. Since NiO is less stable than Cr_2O_3, it supplies oxygen and its dissociation pressure, which is sufficiently high to react with chromium to produce Cr_2O_3. Continuous increase of Cr_2O_3 mainly comes from three sources: Cr rich powder particles reacting with oxygen; $NiCr_2O_4$ decomposing to generate Cr_2O_3 and Cr oxidised by NiO.

Metallic phases of the HVOLF coating undergo rapid transformation to α-Cr only after 1 hour of heat treatment. The α-Cr phase comes out of the Ni-Cr solid solution during the heat treatment. According to the Ni-Cr binary phase diagram Ni phase with Cr content about 34 wt. % and the Cr phase with about 2.4 wt. % is in equilibrium at 700 ℃ [11]. The Rietveld analysis also indicates that a small amount of Ni (3 - 4 %) appears after 10 h. As the Cr precipitated out of the NiCr solution a pure Ni phase was created. The disappearance of the α-

Cr peak at 100 h is due to the formation of Cr depleted region, which is around 5 μm, underneath the oxide scale. Cr_2O_3 is an outward growing oxide and oxidation of Cr occurs by outward migration of Cr ion toward the scale-gas boundary. The oxidation of the HVOLF coating progresses through the formation of a thin Cr_2O_3 layer. The Cr_2O_3 peaks increase in intensity with increasing exposure time and a small amount of NiO and $NiCr_2O_4$ grow after a longer exposure. NiO is formed from the splats depleted in Cr and NiO reacts with Cr_2O_3 to form $NiCr_2O_4$. Cr_2O_3 is a protective oxide scale which can prevent the coating from further oxidation and this provides suitable protection to the underlying substrate. In many high temperature engineering applications, the coating relies on this protective oxide scale and hence, understanding the kinetics and mechanism of the oxidation of this coating is crucial.

In this study, the HVOLF coatings showed better oxidation performance due to lower levels of oxides and porosity; although it is difficult to isolate which one is more influential on the oxidation performance. For both coatings, optimised spray parameters were used to deposit commercial grade coatings for industrial applications and hence the aim of this study was to compare the oxidation performance of a typical HVOLF versus HVOGF sprayed Ni50Cr coating. Another study is currently underway to investigate the role of oxide content and the porosity in the oxidation/ corrosion performance of the coatings, which will be reported in due course.

5. Conclusions

In this study, Ni50Cr feedstock powder was deposited using HVOGF and HVOLF thermal spray onto a modified 9Cr (ASME P92) boiler steel. The microstructure and porosity of the coatings were examined in detail. The high temperature oxidation kinetics of the coatings was examined in short term TGA in air and the phase evolution of the coatings was studied in longer term air oxidation test using XRD Rietveld method. . Following conclusions can be drawn:

- HVOGF coatings contain much more oxides due to higher particle melting during the spraying process than that of HVOLF coating. The as-sprayed HVOGF coating contained NiO, Cr_2O_3 and $NiCr_2O_4$ oxides and elemental Ni along with γ - (Ni, Cr) solid solution. No oxides were detected in the HVOLF coating in the XRD and the coating was mainly composed of γ - (Ni, Cr) and α-Cr.

- HVOGF sprayed deposit also contained higher level of inter-connected porosity. The pores in HVOGF coatings had wider size range distribution than that of the HVOLF coatings. The pores in the HVOLF coatings were mostly at the splat boundaries and were in the range of 0.06 - 0.3 µm.

- In TGA experiments, a two-stage parabolic oxidation kinetics was observed in both coatings. The parabolic rate constants and the overall mass gain for HVOGF were higher than those of HVOLF coating. Higher oxide content and high levels of porosity in the HVOGF coating resulted in lower oxidation resistance at high temperature oxidation.

- In both samples, oxide scales covered the coating surface after 100 h exposure in air at 700 ℃; However, the size of oxide grains in HVOLF was much larger and the well-defined.

- The main oxide generated at the surface of coatings after 100 h exposure for two coatings is mainly Cr_2O_3; but, the mechanisms of oxidation are quite different. In HVOLF coating, the main contributor for Cr_2O_3 is the oxidation of Cr element in the alloy; whereas, in HVOGF coating, along with oxidation of Cr, $NiCr_2O_4$ decomposed to generate Cr_2O_3 and Cr was also oxidised by NiO.

References

[1] T. Hussain, T. Dudziak, N. Simms, J. Nicholls, Fireside corrosion behavior of HVOF and plasma-sprayed coatings in advanced coal/biomass co-fired power plants, J. Therm. Spray Technol., 22 (2013) 797-807.

[2] M. Oksa, P. Auerkari, J. Salonen, T. Varis, Nickel-based HVOF coatings promoting high temperature corrosion resistance of biomass-fired power plant boilers, Fuel Process. Technol., 125 (2014) 236-245.

[3] S. Bluni, A. Marder, Effects of thermal spray coating composition and microstructure on coating response and substrate protection at high temperatures, Corrosion, 52 (1996) 213-218.

[4] H. Al-Fadhli, J. Stokes, M. Hashmi, B. Yilbas, The erosion–corrosion behaviour of high velocity oxy-fuel (HVOF) thermally sprayed inconel-625 coatings on different metallic surfaces, Surf. Coat. Technol., 200 (2006) 5782-5788.

[5] M. Uusitalo, P. Vuoristo, T. Mäntylä, High temperature corrosion of coatings and boiler steels in reducing chlorine-containing atmosphere, Surf. Coat. Technol., 161 (2002) 275-285.

[6] T. Sundararajan, S. Kuroda, T. Itagaki, F. Abe, Steam oxidation resistance of Ni-Cr thermal spray coatings on 9Cr-1Mo steel. Part 2: 50Ni-50Cr, ISIJ int., 43 (2003) 104-111.

[7] H. Edris, D. McCartney, A. Sturgeon, Microstructural characterization of high velocity oxy-fuel sprayed coatings of Inconel 625, J Mater Sci, 32 (1997) 863-872.

[8] J.R. Davis, Handbook of thermal spray technology, ASM international 2004.

[9] D. Agarwal, W. Herda, U. Brill, Nickel alloys combat high-temperature corrosion, Adv. Mater. Processes, 148 (1995).

[10] N. Birks, G.H. Meier, F.S. Pettit, Introduction to the high temperature oxidation of metals, Cambridge University Press2006.

[11] H. Baker, H. Okamoto, Alloy phase diagrams, ASM International, ASM Handbook., 3 (1992) .

[12] K. Strafford, P. Datta, Design of sulphidation resistant alloys, Mater. Sci. Technol., 5 (1989) 765-779.

[13] D. Zhang, S.J. Harris, D.G. McCartney, Microstructure formation and corrosion behaviour in HVOF-sprayed Inconel 625 coatings, Mater. Sci. Eng., A, 344 (2003) 45-56.

[14] T. Monecke, S. Köhler, R. Kleeberg, P.M. Herzig, J.B. Gemmell, Quantitative phase-analysis by the Rietveld method using X-ray powder-diffraction data: application to the study of alteration halos associated with volcanic-rock-hosted massive sulfide deposits, Can. Mineral., 39 (2001) 1617-1633.

[15] B.D. Cullity, Elements of X-ray Diffraction, (2001).

[16] A. Hewitt, Technology of Oxy-Fuel Gas Processes. Pt. 2. Comparative Combustion Properties of Fuel Gases, Weld. Met. Fab., 40 (1972) 382-390.

[17] P.A. Webb, An introduction to the physical characterization of materials by mercury intrusion porosimetry with emphasis on reduction and presentation of experimental data, Micromeritics Instrument Corp, Norcross, Georgia, (2001).

[18] M.A. Laskar, R. Kumar, B. Bhattacharjee, Some aspects of evaluation of concrete through mercury intrusion porosimetry, Cem. Concr. Res., 27 (1997) 93-105.

[19] G. Calvarin, R. Molins, A. Huntz, Oxidation mechanism of Ni—20Cr foils and its relation to the oxide-scale microstructure, Oxid. Met., 53 (2000) 25-48.

[20] E. Essuman, G. Meier, J. Zurek, M. Hänsel, T. Norby, L. Singheiser, W. Quadakkers, Protective and non-protective scale formation of NiCr alloys in water vapour containing high-and low-pO 2 gases, Corros. Sci., 50 (2008) 1753-1760.

[21] B. Kear, F. Pettit, D. Fornwalt, L. Lemaire, On the transient oxidation of a Ni-15Cr-6Al alloy, Oxid. Met., 3 (1971) 557-569.

[22] A. Ul-Hamid, A TEM study of the oxide scale development in Ni-Cr alloys, Anti-Corros. method mater., 51 (2004) 216-222.

[23] T. Sundararajan, S. Kuroda, T. Itagaki, F. Abe, Steam Oxidation Resistance of Ni-Cr Thermal Spray Coatings on 9Cr-1Mo Steel. Part 1: 80Ni-20Cr, ISIJ int., 43 (2003) 95-103.

Table 1 Composition of feedstock powder and substrate (wt. %)

	Fe	Cr	Si	Ni	C	O	Other
Ni50Cr	1	46	2	Bal.	0.1	0.027	1
P92	Bal.	8.91	0.37	0.22	0.11		

Table 2 Process parameters of HVOGF and HVOLF thermal spraying

Parameters	**HVOGF**	**HVOLF**
Oxygen flow rate (l/min)	243	878
Fuel flow rate (l/min)	614 (Hydrogen)	0.445 (Kerosene)
Oxygen stoichiometry (%)	80	100
Gun traverse speed (mm/s)	5	5
Powder feed rate (g/min)	42	72
Carrier gas flow rate (l/min)	6	6
Stand-off distance (mm)	254	355
No of passes	10	10

Table 3 Phase compositions (wt. %) measured with Rietveld of the as-sprayed and exposed coatings after 1, 10 and 100 h

Phase	**Ni50Cr powder**	**HVOGF**				**HVOLF**			
		As-sprayed	1 h	10 h	100 h	As-sprayed	1 h	10 h	100 h
γ-(Ni, Cr)	96.0	28.1	40.4	41.1	42.2	94.0	65.1	57.0	43.3
α-Cr	4.0					3.3	20.8	15.4	
Ni		23.7	16.8	11.8	3.9			3.7	4.4
Cr_2O_3		5.2	30.5	38.5	43.6		11.8	19.3	42.4
$NiCr_2O_4$		31.1	8.4	6.3	8.0			2.8	7.4
NiO		8.1	3.9	2.4	2.4				2.5

Figure 1 Schematic illustration of setup of HVOGF and HVOLF guns [13]

Figure 2 XRD patterns of feedstock powder and as-sprayed HVOGF and HVOLF coatings

Figure 3 SEM images of a. as-received powder particles morphology; b. polished cross-section

Figure 4 SEM images of cross-section of as-sprayed coating: a. HVOGF coating at low magnification; b. HVOGF coating at high magnification showing porosity; c. HVOLF coating at low magnification; d. HVOLF coating at high magnification showing inter-splat boundaries

Figure 5 SEM images of top morphology of two coatings: a. HVOGF coating; b. HVOLF coating showing various degree of particle melting

Figure 6 Incremental intrusion of mercury versus pore size of HVOGF and HVOLF free standing deposits

Figure 7 Cumulative intrusion of mercury versus pore size of HVOGF and HVOLF free standing deposits

Figure 8 TGA curves of two free standing deposits at 700 ℃ for 240 minutes

Figure 9 Kinetics of two free standing deposits at 700 ℃

Figure 10 XRD patterns of HVOGF coating after exposure at 700 ℃ for 1, 10 and 100 h

Figure 11 XRD patterns of HVOLF coating exposure at 700 ℃ for 1, 10 and 100 h

Figure 12 SE images of the morphology of the oxide whiskers at the top surface of the coatings exposed at 700 ◦C for 100 h: a. HVOGF coating at low magnification; b. HVOGF coating at high magnification showing oxide grains; c. HVOLF coating at low magnification; d. HVOLF coating at large magnification showing much larger oxides

Figure 13 BSE cross-section images of the HVOGF coating (a-c) and HVOLF coating (d-f) after 100 h; a & d. overall image of the coating cross-section; b & d. high magnification image of the oxidation products; c & f. high magnification image of the coating microstructure.

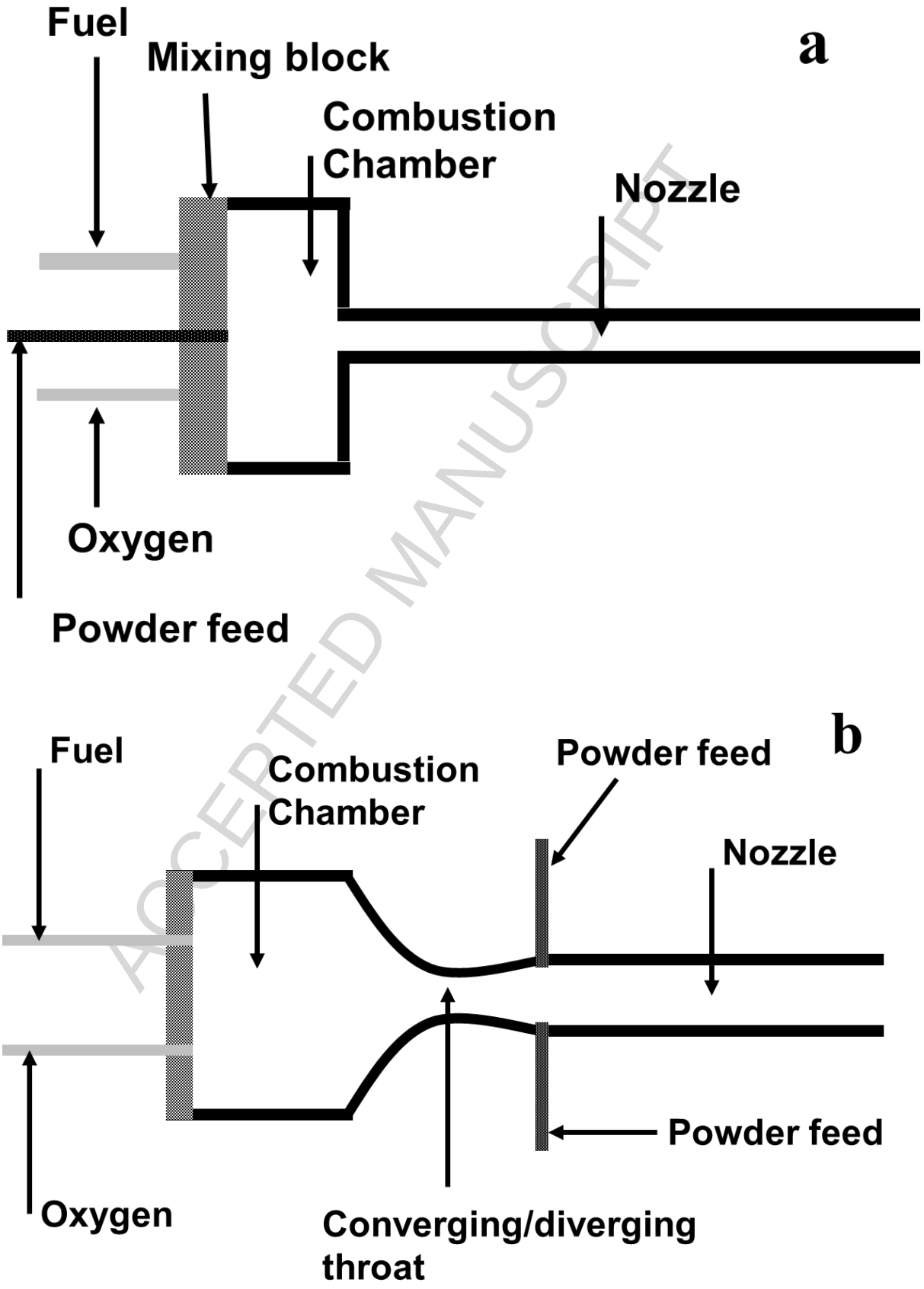

Figure 1 Schematic illustration of setup of HVOGF (a) and HVOLF guns (b) [13]

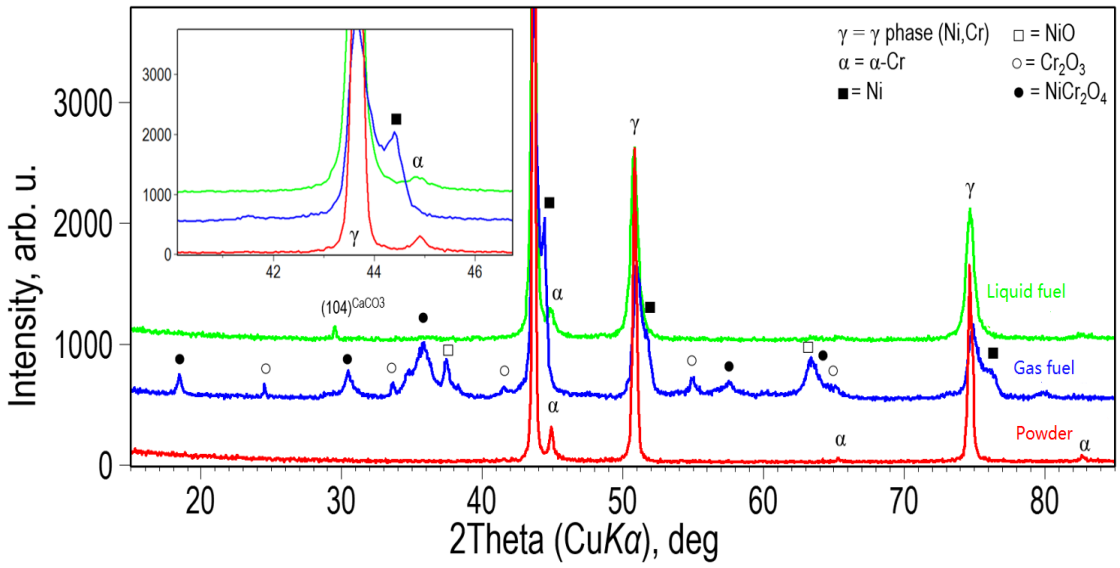

Figure 2 XRD patterns of feedstock powder and as-sprayed HVOGF and HVOLF coatings

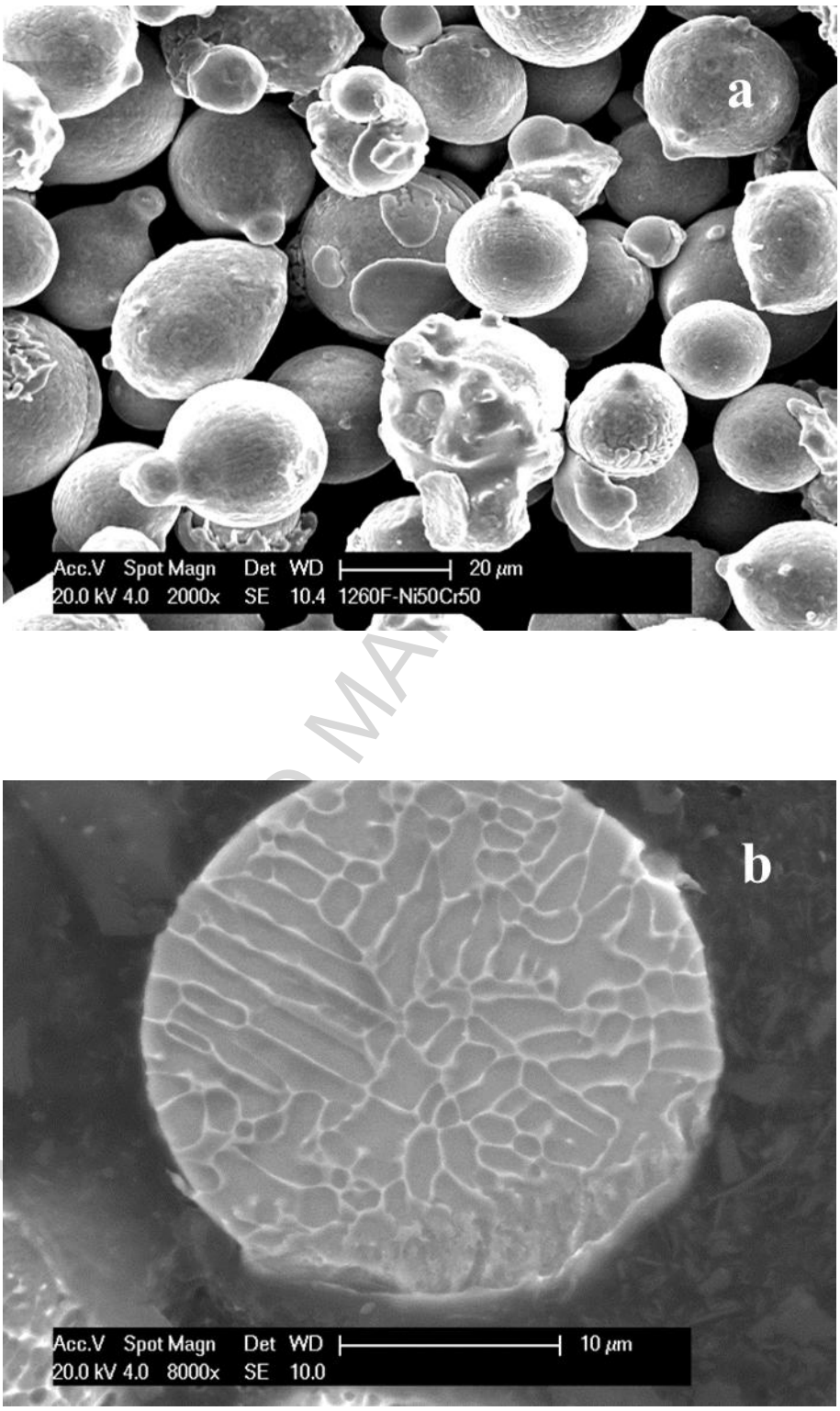

Figure 3 SEM images of a. as-received powder particles morphology; b. polished cross-section

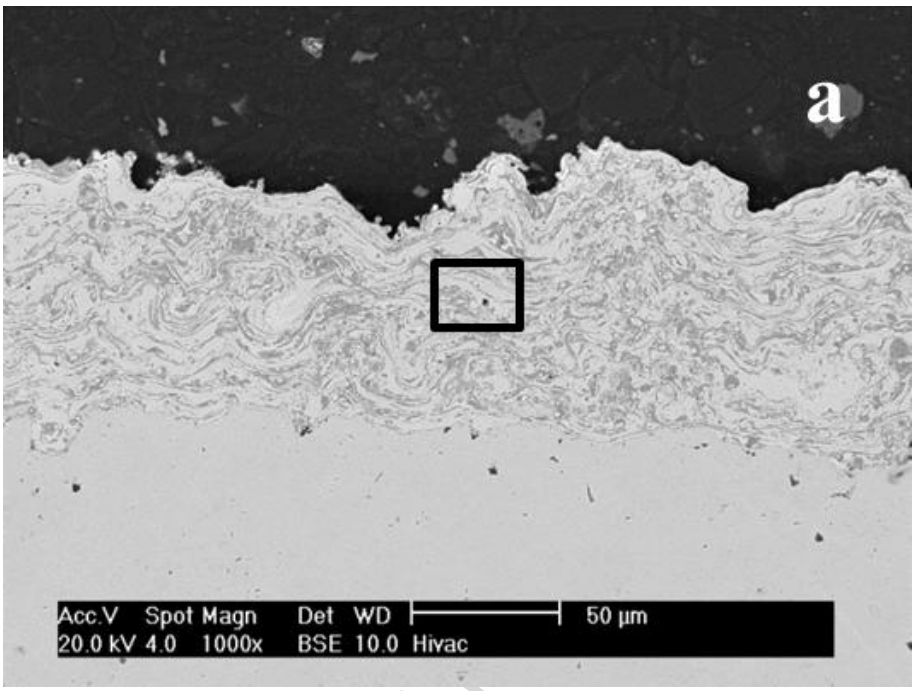

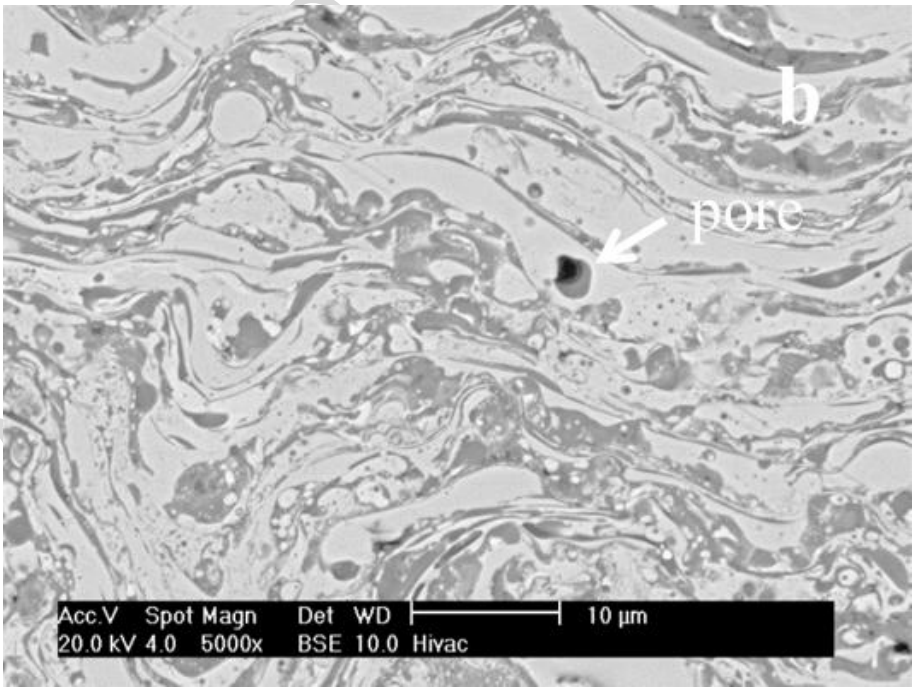

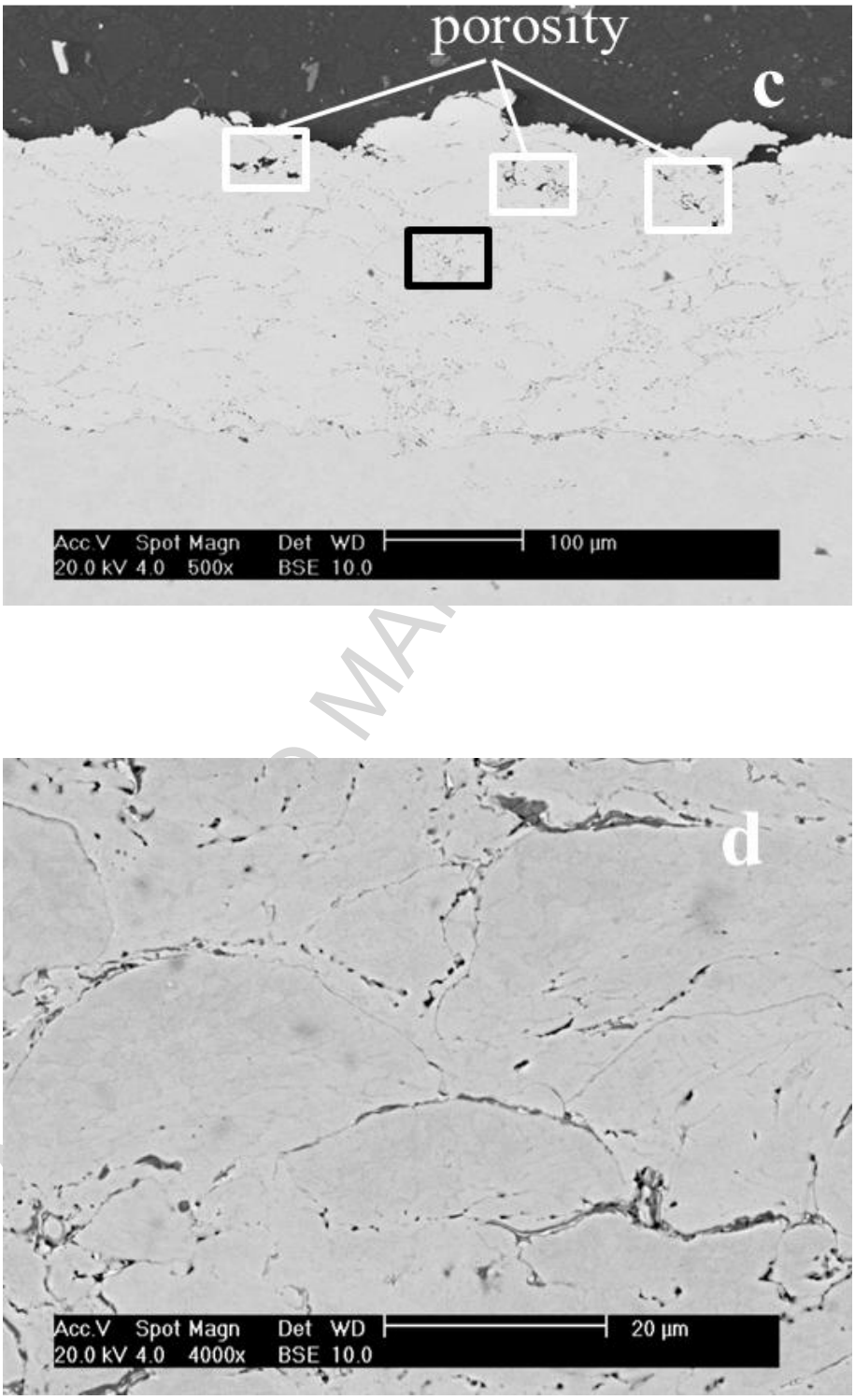

Figure 4 SEM images of cross-section of as-sprayed coating: a. HVOGF coating at low magnification; b. HVOGF coating at high magnification showing porosity; c. HVOLF coating at low magnification; d. HVOLF coating at high magnification showing inter-splat boundaries

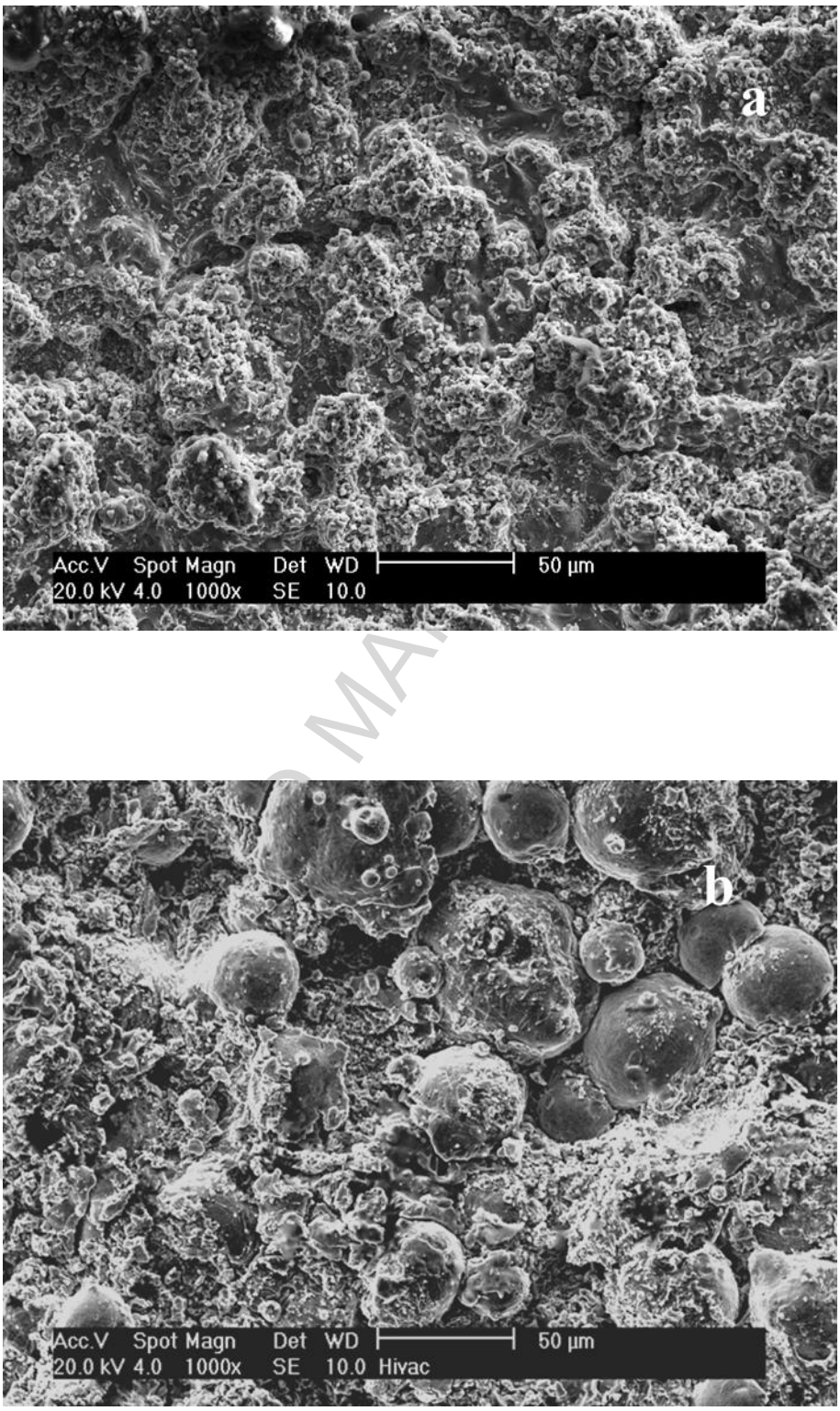

Figure 5 SEM images of top morphology of two coatings: a. HVOGF coating; b. HVOLF coating showing various degree of particle melting

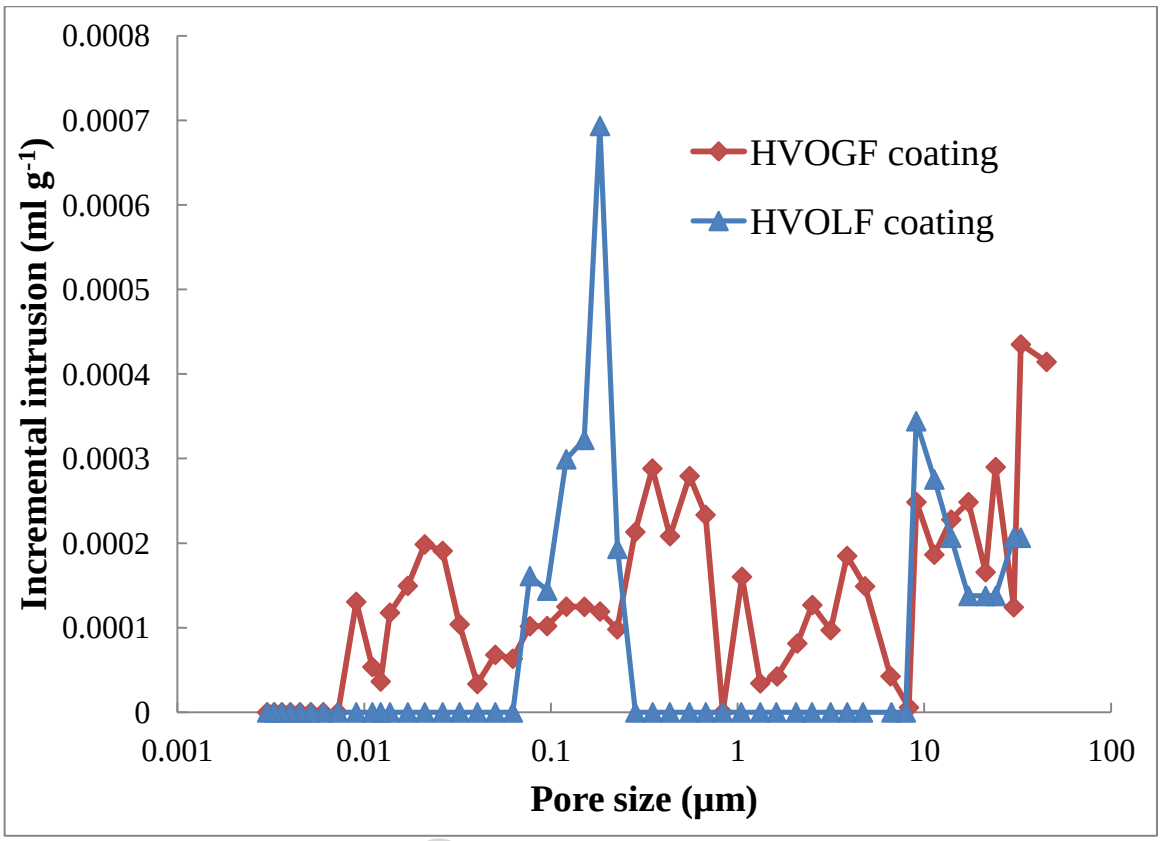

Figure 6 Incremental intrusion of mercury versus pore size of HVOGF and HVOLF free standing deposits

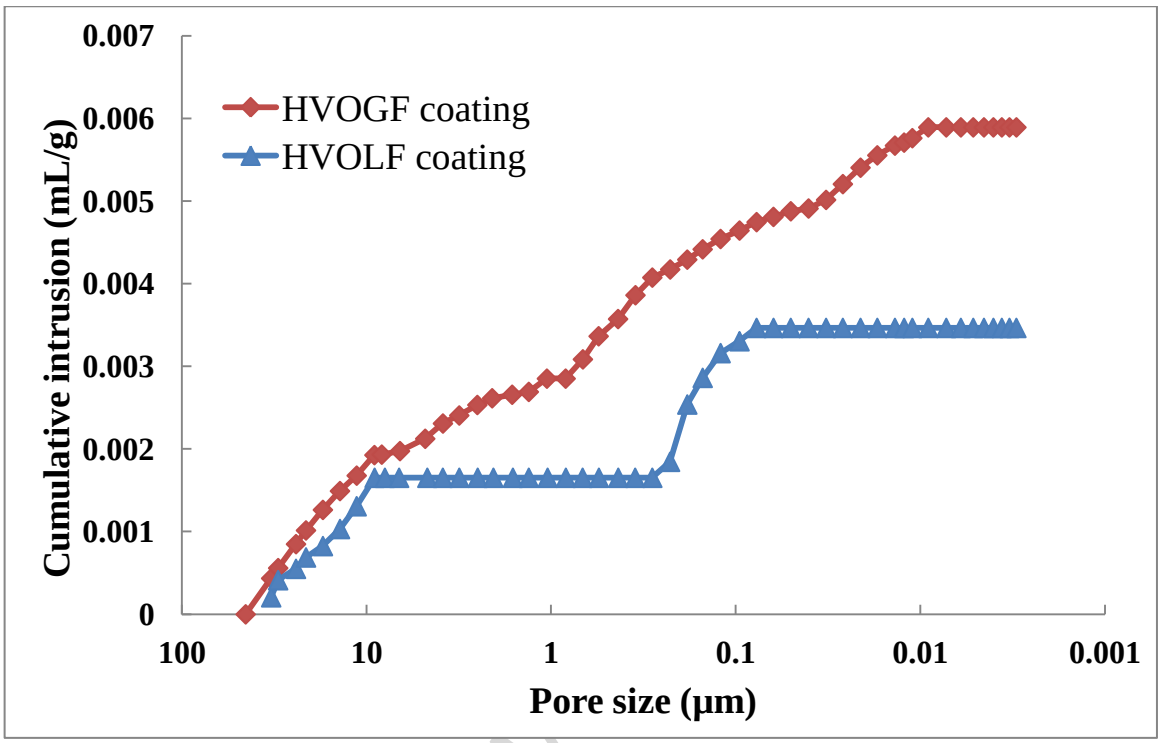

Figure 7 Cumulative intrusion of mercury versus pore size of HVOGF and HVOLF free standing deposits

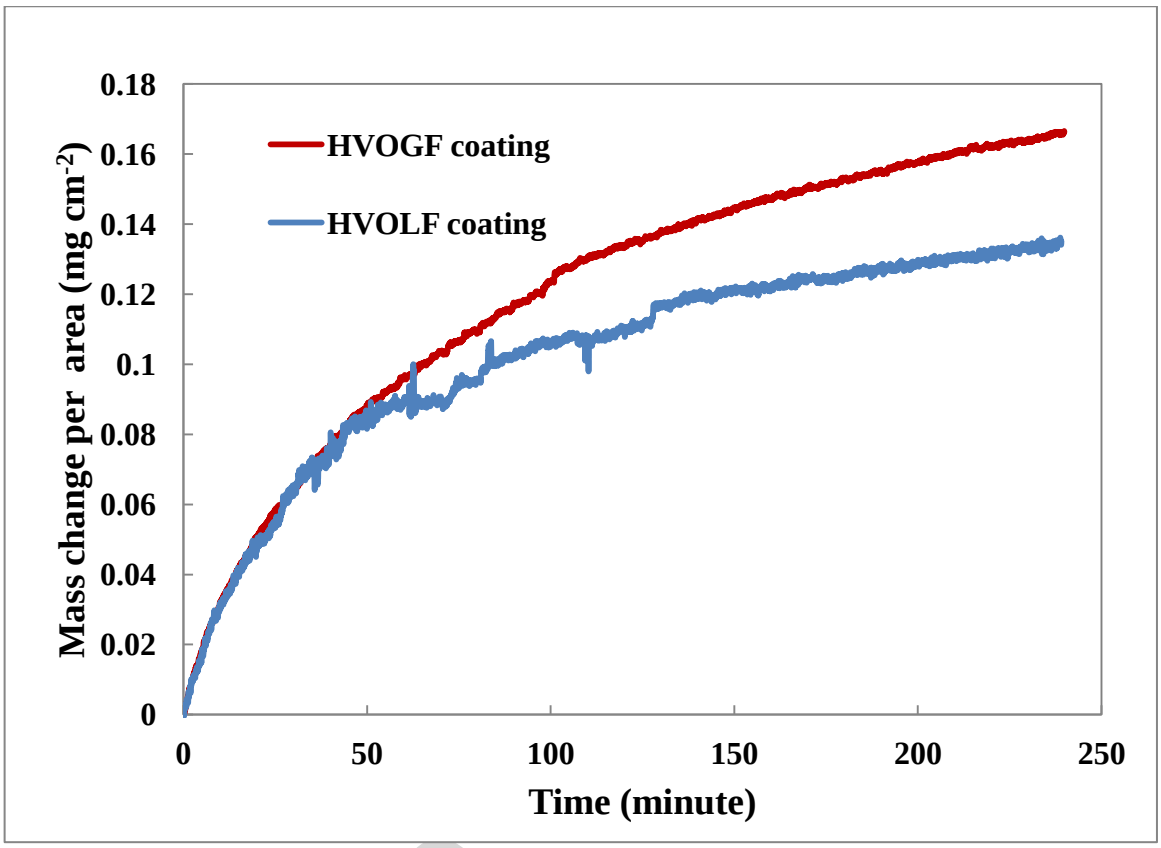

Figure 8 TGA curves of two free standing deposits at 700 ℃ for 240 minutes

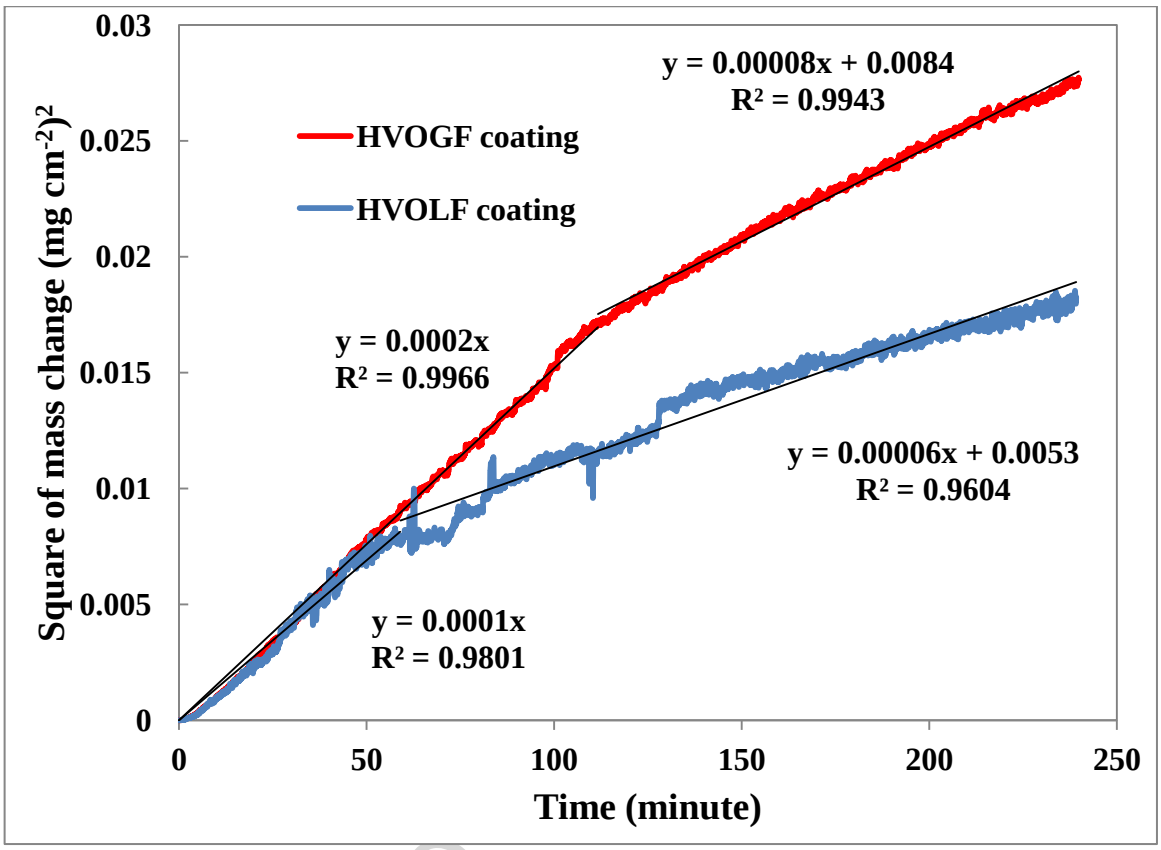

Figure 9 Kinetics of two free standing deposits at 700 ℃

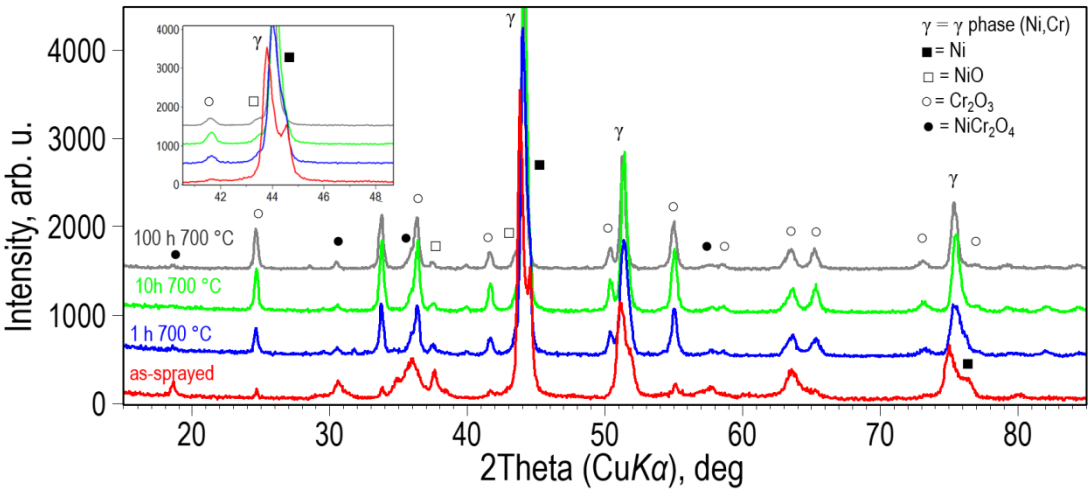

Figure 10 XRD patterns of HVOGF coating after exposure at 700 ℃ for 1, 10 and 100 h

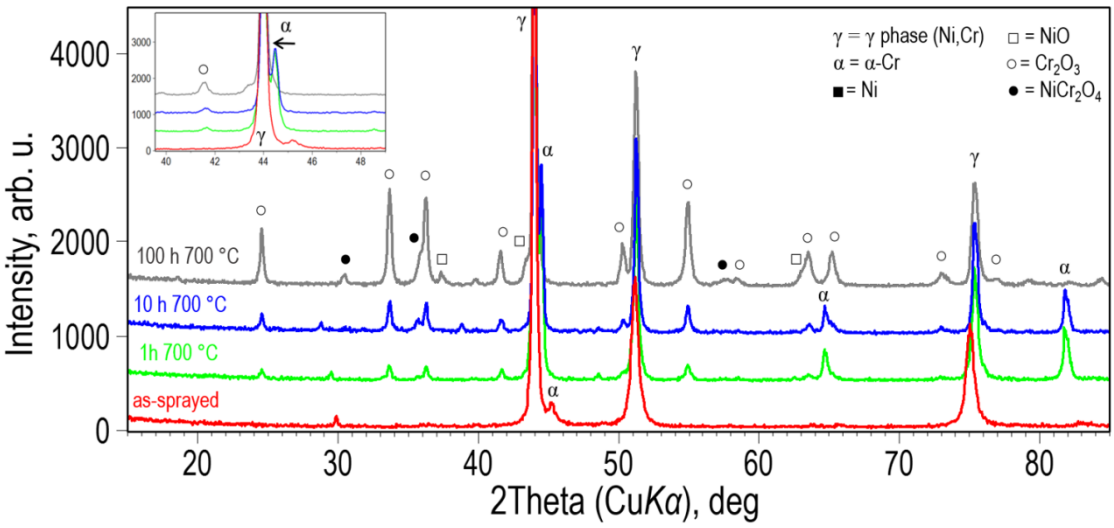

Figure 11 XRD patterns of HVOLF coating exposure at 700 ℃ for 1, 10 and 100 h

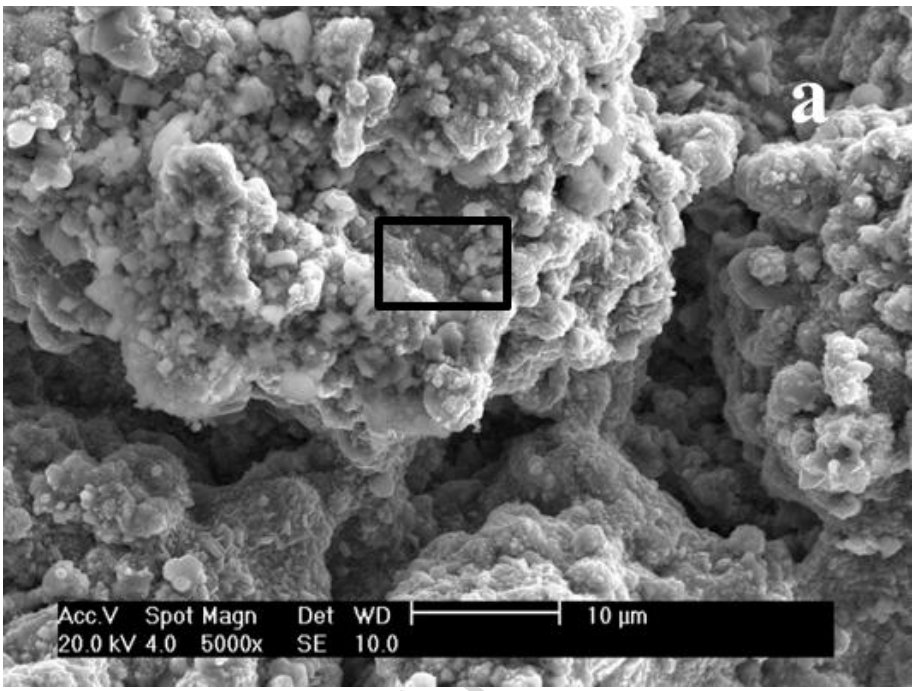

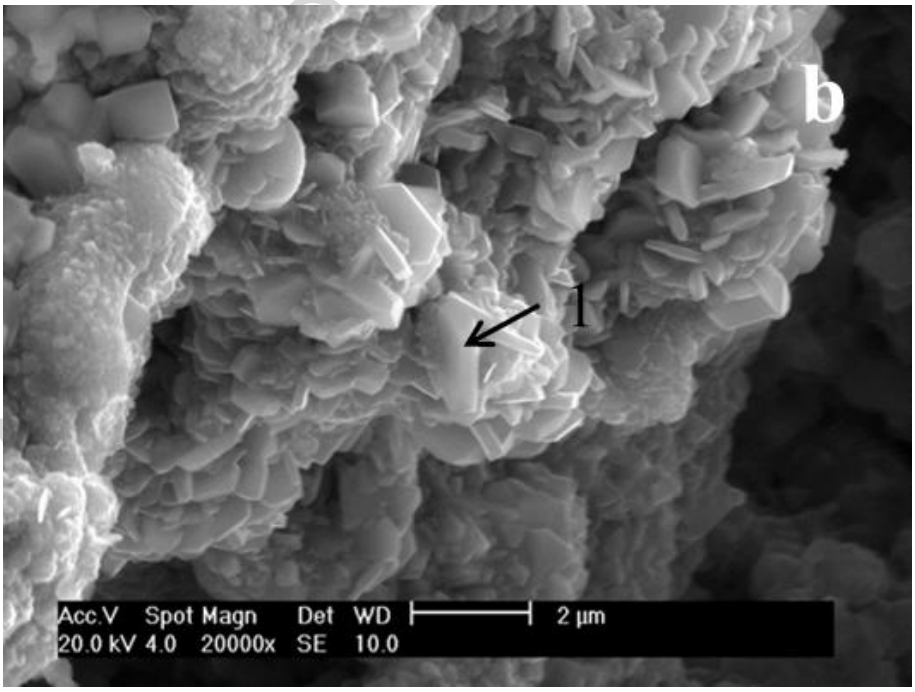

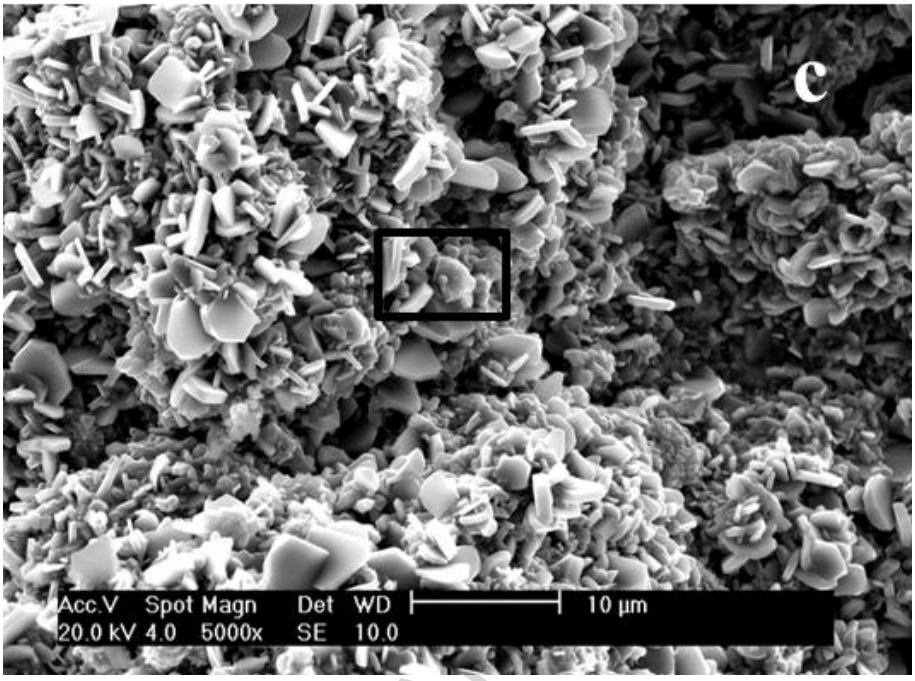

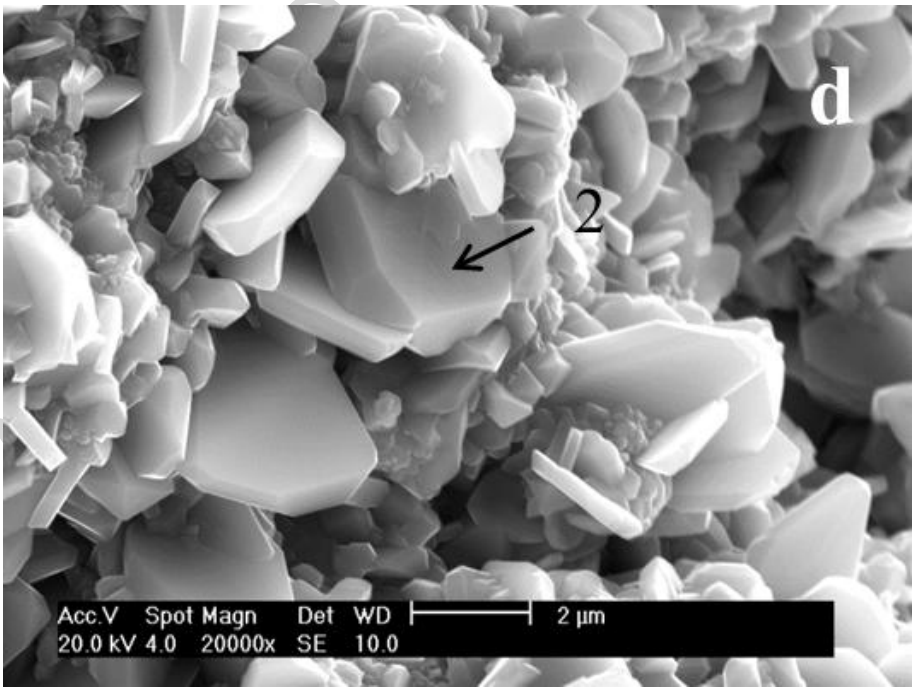

Figure 12 SE images of the morphology of the oxide whiskers at the top surface of the coatings exposed at 700 ◦C for 100 h: a. HVOGF coating at low magnification; b. HVOGF coating at high magnification showing oxide grains; c. HVOLF coating at low magnification; d. HVOLF coating at large magnification showing much larger oxides

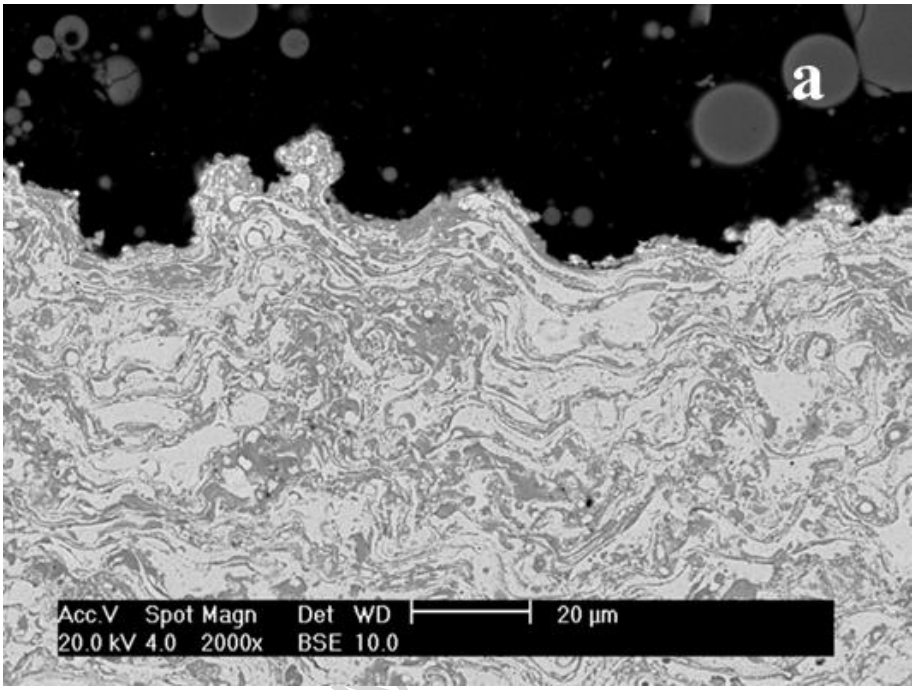

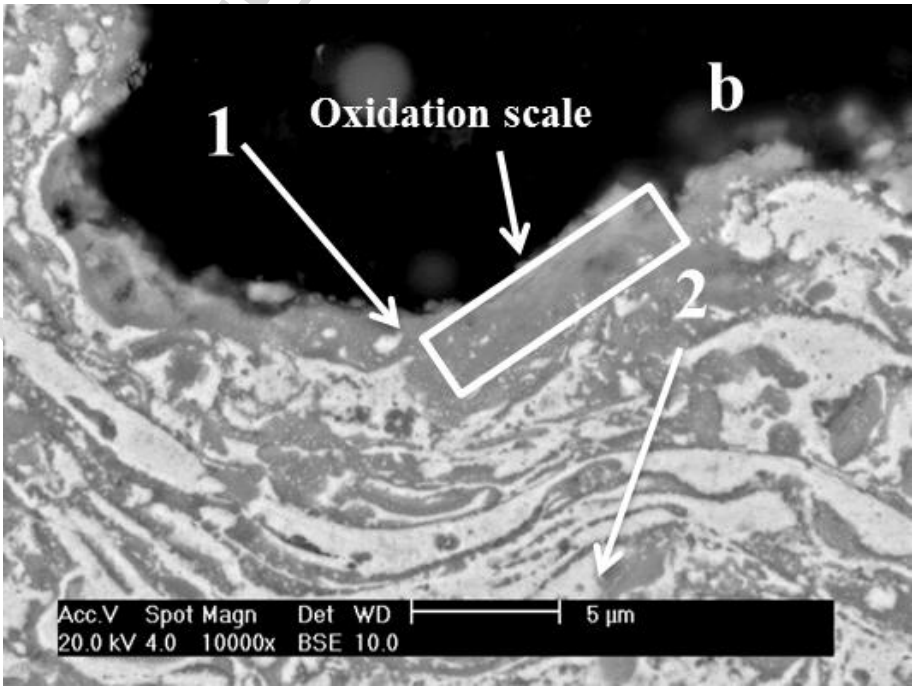

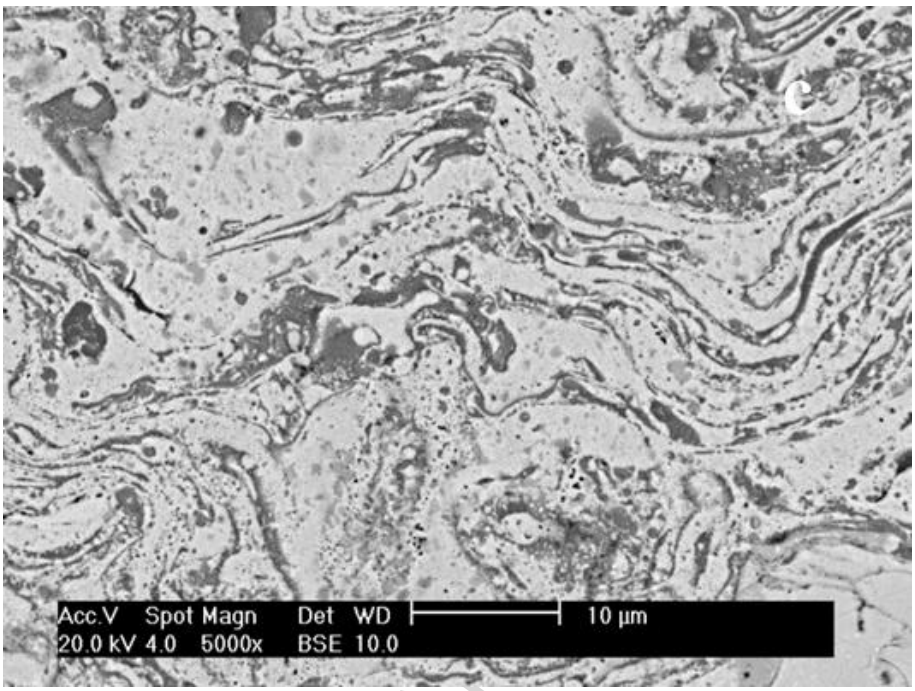

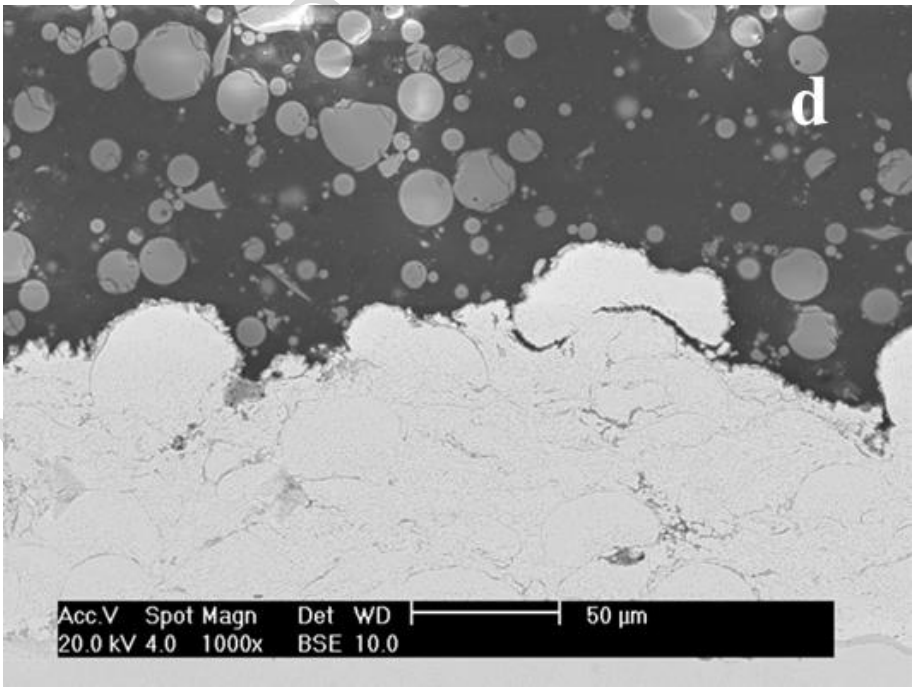

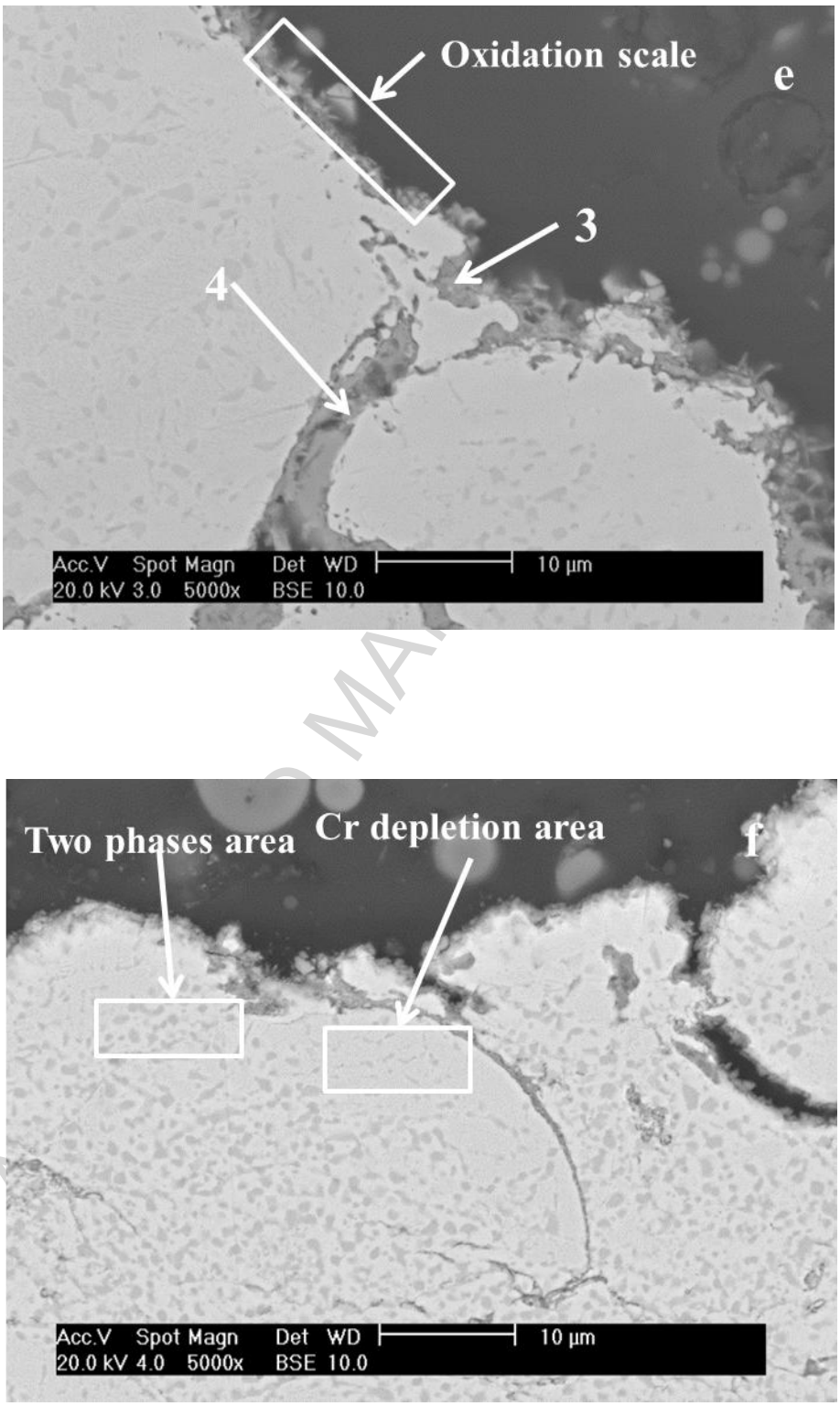

Figure 13 BSE cross-section images of the HVOGF coating (a-c) and HVOLF coating (d-f) after 100 h; a & d. overall image of the coating cross-section; b & d. high magnification image of the oxidation products; c & f. high magnification image of the coating microstructure.

Highlights

- HVOGF coatings contains γ, Ni, oxide phases and HVOLF contains only γ and Cr phases
- Oxygen level and porosity of HVOGF are both larger than that of HVOLF coating
- HVOLF brings about better high temperature oxidation resistance to Ni50Cr coating than HVOGF
- Oxidation of both coatings at 700 ℃ follow a two stage parabolic law
- Oxidation products of both coatings after 100 h heattreament is same in types and composition: 40 wt% Cr_2O_3 and 10 wt % NiO with $NiCr_2O_4$